

Supplement to ‘Sigmoidal water retention function with improved behavior in dry and wet soils’

Generating weather records for monsoon, semi–arid, and temperate climates

The weather generator TEmpotRain (de Rooij, 2018) was used to generate 1000–year records of daily rainfall, temperature (daily mean, minimum, and maximum), solar radiation, and daily potential evapotranspiration (ET_{pot}). The latter was calculated from the solar radiation and the temperatures according to de Rooij’s (2018) version of the modified Hargreaves equation (Droogers and Allen, 2002). Droogers and Allen (2002) showed that their modification (which takes into account the monthly rainfall sums) improves the results, especially for drier climates. De Rooij (2018) used the rainfall sum in a 30–day moving time window instead of monthly sums. He also implemented Evett’s (2000, p. A150) temperature correction that accounts for the energy that is used to warm up the soil water and therefore is not available to turn liquid water into vapor.

The weather statistics to characterize the three climates (Table 1 in the main text) are based on the 1000–year records. The numerical simulations of soil water flow were carried out with the first 16 years of these records.

The weather generator (de Rooij, 2018) requires input parameters that define the weather that needs to be generated. The rainfall parameters for the monsoon climate are given in Table S1, those for the semi–arid climate in Table S2, and those for the temperate climate in Table S3. The parameters governing the temperature and ET_{pot} for all climates are listed in Table S4. De Rooij (2018) explains the meaning and purpose of the various parameters. Tables S1–S3 follow the notation of Table 1 of de Rooij (2018). In cases where the symbols used there are used for other variable in this paper they have the subscript ‘wg’ in this supplement to indicate they relate to the weather generator. Table S4 follows the notation of Table 5 in de Rooij (2018).

Table S1. The parameters governing rainfall of the monsoon climate.

Period	Start time (d)	λ_{wg} (d ⁻¹)	ρ	δ (d mm ⁻¹)	α_{wg}	ν (d)	κ	φ	ε (d ⁻¹)
1	0.0	0.300	1.50	0.0124	1.50	0.0156	0.750	0.250	6.91
2	60.0	0.578	1.50	0.0357	1.80	0.188	1.25	0.625	4.61
3	152.0	0.575	1.60	0.0320	2.00	0.100	0.600	0.300	9.21
4	274.0	0.667	1.20	0.0522	1.20	0.100	2.00	0.333	3.84
5	335.0	0.300	1.50	0.0124	1.50	0.0156	0.750	0.250	6.91

Table S2. The parameters governing rainfall of the semi–arid climate.

Period	Start time (d)	λ_{wg} (d ⁻¹)	ρ	δ (d mm ⁻¹)	α_{wg}	ν (d)	κ	φ	ε (d ⁻¹)
1	0.0	0.060	1.20	0.0233	1.50	0.0313	1.50	0.500	6.14
2	106.0	0.350	1.80	0.0356	4.00	0.167	2.00	0.500	6.14
3	213.0	0.567	1.50	0.0564	2.00	0.167	2.00	0.500	4.61
4	281.0	0.060	1.20	0.0233	1.50	0.0313	1.50	0.500	6.14

34 The rainfall data for the temperate climate were taken from the literature (Pham
 35 et al., 2013). The other weather parameters were fitted by trial and error to (sometimes
 36 scant) weather data available from various on-line sources for the regions near the cities
 37 of Colombo in Sri Lanka (monsoon climate), Tamale in Ghana (semi-arid climate), and
 38 Ukkel in Belgium (temperate climate). Note that the first and last lines in Tables S1 and
 39 S2 are identical. This indicates that one of the periods for which rainfall generator
 40 parameters needed to be specified started late in the year and continued into the next
 41 year.

42
 43 Table S3. The parameters governing rainfall of the temperate climate (Pham et al., 2013).

Period	λ_{wg} (d ⁻¹)	p	δ (d mm ⁻¹)	α_{wg}	ν (d)	κ	φ	ε (d ⁻¹)
Jan	0.768	2.304	0.0680	3.000	0.0320	0.200	0.046	1.52E-14
Feb	0.672	2.663	0.0777	3.000	0.0316	0.193	0.044	2.22E-14
Mar	0.648	1.463	0.0413	3.000	0.0268	0.223	0.044	1.38E-14
Apr	0.648	2.525	0.0525	3.000	0.0196	0.157	0.030	6.00E-14
May	0.576	0.696	0.0290	3.788	0.0274	0.167	0.035	4.08E-12
Jun	0.552	0.654	0.0273	5.292	0.0458	0.162	0.035	6.05
Jul	0.576	0.429	0.0179	5.893	0.0448	0.149	0.030	11.1
Aug	0.672	0.716	0.0298	3.000	0.0151	0.217	0.046	2.93E-13
Sep	0.600	0.923	0.0385	3.000	0.0179	0.176	0.035	1.02E-13
Oct	0.552	1.523	0.0635	3.000	0.0343	0.166	0.038	3.82E-14
Nov	0.696	1.519	0.0633	3.000	0.0343	0.190	0.040	1.72E-13
Dec	0.720	1.936	0.0807	3.000	0.0373	0.180	0.043	2.25E-14

44
 45
 46 Table S4. Parameters for the temperature, cloudiness, and evapotranspiration. The
 47 parameters are explained in de Rooij (2018, Table 5).

Parameter	Monsoon climate	Semi-arid climate	Temperate climate
\bar{T}_a (°C)	27.2	27.9	10.6
σ_T (°C)	2.0	4.0	0.0
A_c (°C)	1.1	2.02	6.0
A_o (°C)	0.7	1.0	3.0
σ_a (°C)	0.20	0.20	2.5
ψ (d)	-48.7	29.7	-122
ϕ	0.60	0.6	0.6
σ_m (°C)	0.20	0.20	2.0
μ_f	1.89	1.76	1.19
$\sigma_{f,c}$	0.16	0.25	0.29
$\sigma_{f,o}$	0.10	0.074	0.15
P_l (mm)	2.0	2.0	2.0
P_h (mm)	50.0	60.0	20.0
f_1	0.10	0.01	0.25
f_2	0.60	0.20	0.95
f_3	0.95	0.30	0.35
Latitude (rad)	0.1190	0.1658	0.8866

49 **Model simulations to test the performance of different parameterizations of**
50 **the soil water retention curve**

51

52 The simulations assumed a grass cover of 10 cm height in all cases. We realize
53 this is not realistic for the semi-arid climate but kept the soil cover the same for all
54 climates to facilitate the comparison between soils and climates. Roots were uniformly
55 distributed in a 50 cm root zone, roughly representative for several grasses (e.g., Brown
56 et al., 2010). For simplicity, interception was neglected. Surface ponding was allowed up
57 to a depth of 1.0 cm. The soil was uniform over the simulation depth of 2.00 m, with a
58 unit-gradient lower boundary condition. Heat flow and vapor flow were not considered.

59 The three soils used in the simulations and the values of their parameters are
60 given in Table 2 of the main text. The acronyms for the parameterizations used here, as
61 well as their equations, are also given in the main text.

62 The initial time step of the numerical solution was 0.001 d. The parameters
63 governing the incremental increase and decrease of the time step were set to the default
64 values, while the parameters of the convergence criteria were set to the values
65 recommended in the manual (Šimůnek et al., 2013, p. 189). The nodal distance was
66 smallest near the surface (4 mm), and gradually increased to reach 19 mm in the region
67 below the root zone. In the lower 5 cm of the profile, the nodal distance decreased
68 gradually to 11 mm at the bottom. The total number of nodes was 151. The simulated
69 period was 16 years. For the analysis that follows, only the final six years were
70 considered in order to minimize the effect of the initial conditions.

71 Initially, the soil was at hydrostatic equilibrium with the groundwater level at 2.00
72 m depth. The upper boundary condition gave the daily precipitation rate during rainy
73 days, converted to a sinusoidal function internally by Hydrus-1D. During dry days, the
74 matric potential at the soil surface was not allowed to fall below -10^7 cm. Daily values of
75 potential evapotranspiration (ET_{pot}) were also provided on input. The albedo of the grass
76 was set to 0.23 for all soils and climates, in line with reported values (e.g., Davies, 1967;
77 Grant et al., 2000).

78 The partitioning of daily ET_{pot} as generated by TEmptRain into daily potential
79 evaporation (E_{pot}) and transpiration (T_{pot}) was done internally by Hydrus-1D. The leaf
80 area index (LAI) was set to 2.4 for grass of the selected height (Šimůnek et al., 2013, p.
81 229). From that the model calculated the soil cover fraction (SCF) as (Šimůnek et al., 2013,
82 p. 229)

83

$$84 \text{SCF} = 1 - e^{-0.463 \text{LAI}} = 0.671 \quad (\text{S1})$$

85

86 The partitioning of ET_{pot} was then straightforward (Šimůnek et al., 2013, p. 38):

87

$$88 T_{pot} = ET_{pot} \text{SCF} = 0.671 ET_{pot} \quad (\text{S2})$$

89

$$90 E_{pot} = ET_{pot} - T_{pot} = 0.329 ET_{pot} \quad (\text{S3})$$

91

92 These daily values were internally converted to low night-time values and higher,
93 sinusoidal daytime values by the model (Šimůnek et al., 2013, p. 38).

94

95 Simulation results

96

97 The monsoon climate represented a region close to the equator (6°49' N lat), and
98 the annual variation in ET_{pot} is therefore limited (Top panels of Fig. S1–S3). The
99 seasonality of the rainfall led to significant drops in E_{act} and T_{act} calculated with RIA during
100 the dry seasons. These drops were more pronounced for clay (Fig. S1) and loamy sand
101 (Fig. S3) than for silt loam (Fig. S2).

102 The values of E_{act} and T_{act} did not differ much between parameterizations for either
103 silt loam (Fig. 4) or loamy sand (Fig. S3), and they ranged in bands whose bounds were
104 dominated more by rainfall than by season. The flow across the lower boundary (deep
105 drainage) was also dominated by rainfall for all three textures (Fig. S1–S3). For silt loam
106 (Fig. S2) deep drainage for VGA was markedly less smooth than for VGN, with RIA in
107 between. The same behavior emerged for loamy sand (Fig. S3), but with an overall
108 reduced damping of the response to the rainfall signal compared to silt loam.

109 The semi-arid location was a little farther away from the equator (9°30' N lat) than
110 the monsoon location, and had a wet and a dry season. Potential evapotranspiration was
111 consistently high (Fig. S4–S6, top panels), but the separation between E_{act} and T_{act} for all
112 soils with the RIA parameterization (Fig. S4–S6, top panels) was less pronounced than
113 that for the monsoon climate.

114 For clay, RIA gave near-zero values for E_{act} and T_{act} during the dry seasons (Fig.
115 S4) with short bursts of evapotranspiration after an occasional storm. Deep drainage in
116 clay occurred infrequently, and only during the rainy season (Fig. S4).

117 For silt loam, E_{act} of all three parameterizations dropped sharply at the end of the
118 rainy season, and for some years even during dry periods within the rainy season (Fig.
119 S5). Unsurprisingly, this effect was stronger for loamy sand (Fig. S6). Loamy sand's
120 separation between E_{act} and T_{act} was somewhat more pronounced than that for silt loam.
121 Silt loam allowed transpiration to occur for longer and at a higher rate during the dry
122 season than loamy sand. For both soils, RIA tended to allow higher transpiration rates
123 during the dry season than VGA and VGN.

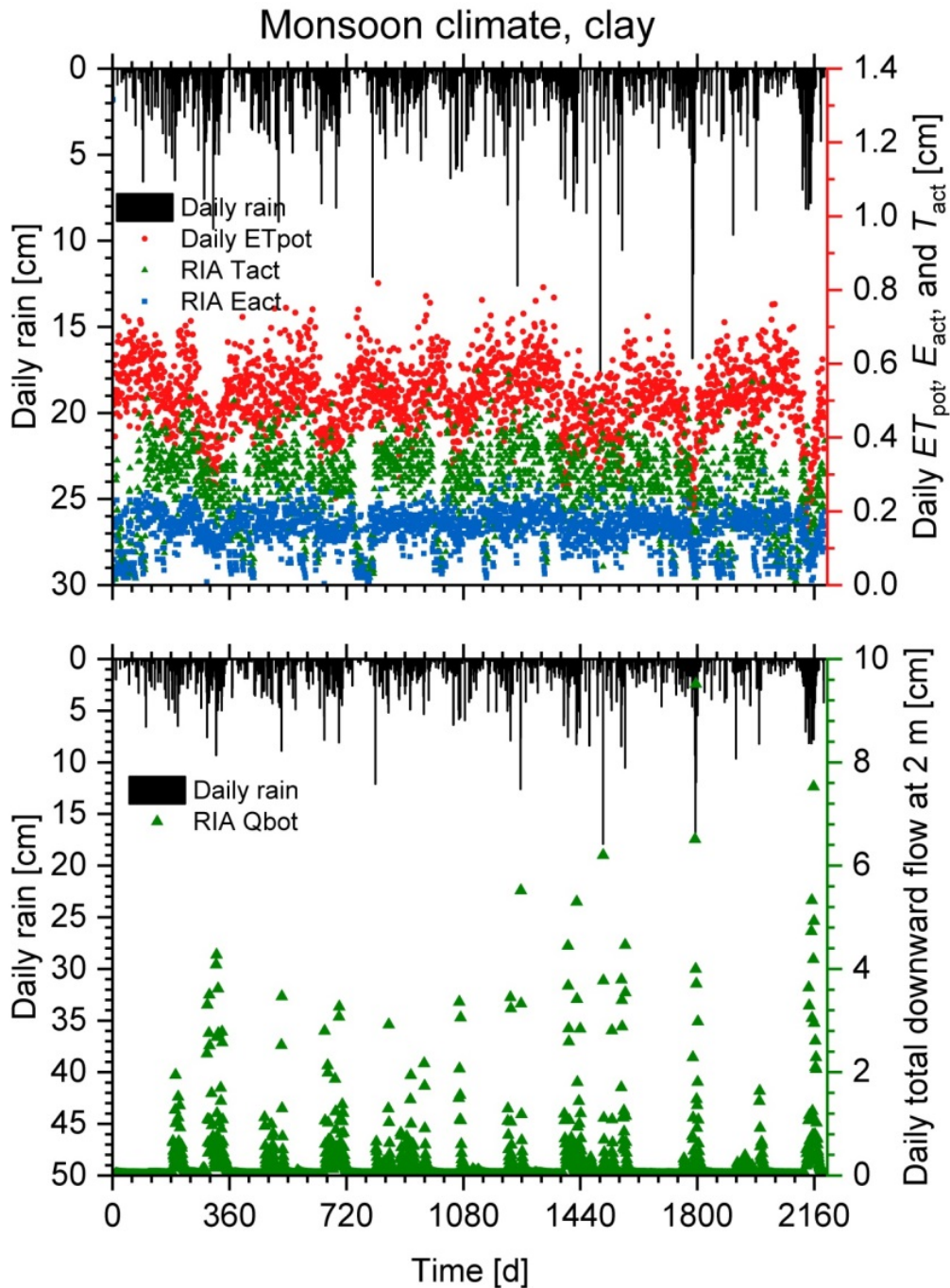
124 Deep drainage was rare in the semi-arid climate, and varied strongly between the
125 years, depending on the annual rainfall. For both silt loam and loamy sand, VGA generated
126 deep drainage more often and at a higher rate than VGN, with RIA in between but much
127 closer to VGN than to VGA (Fig. S4–S6).

128 The location with the moderate climate was far away from the equator (50°48' N
129 lat), resulting in a strong seasonal trend in ET_{pot} (Fig. S7–S9, top panels). There were
130 wetter and drier periods, but no real dry season. For all soils, both E_{act} and T_{act} dropped in
131 winter in response to the very low E_{pot} in that season (Fig. S7–S9). In clay, the rainfall deficit
132 in summer led to a drop in T_{act} in late spring/early summer while E_{act} was affected much
133 less.

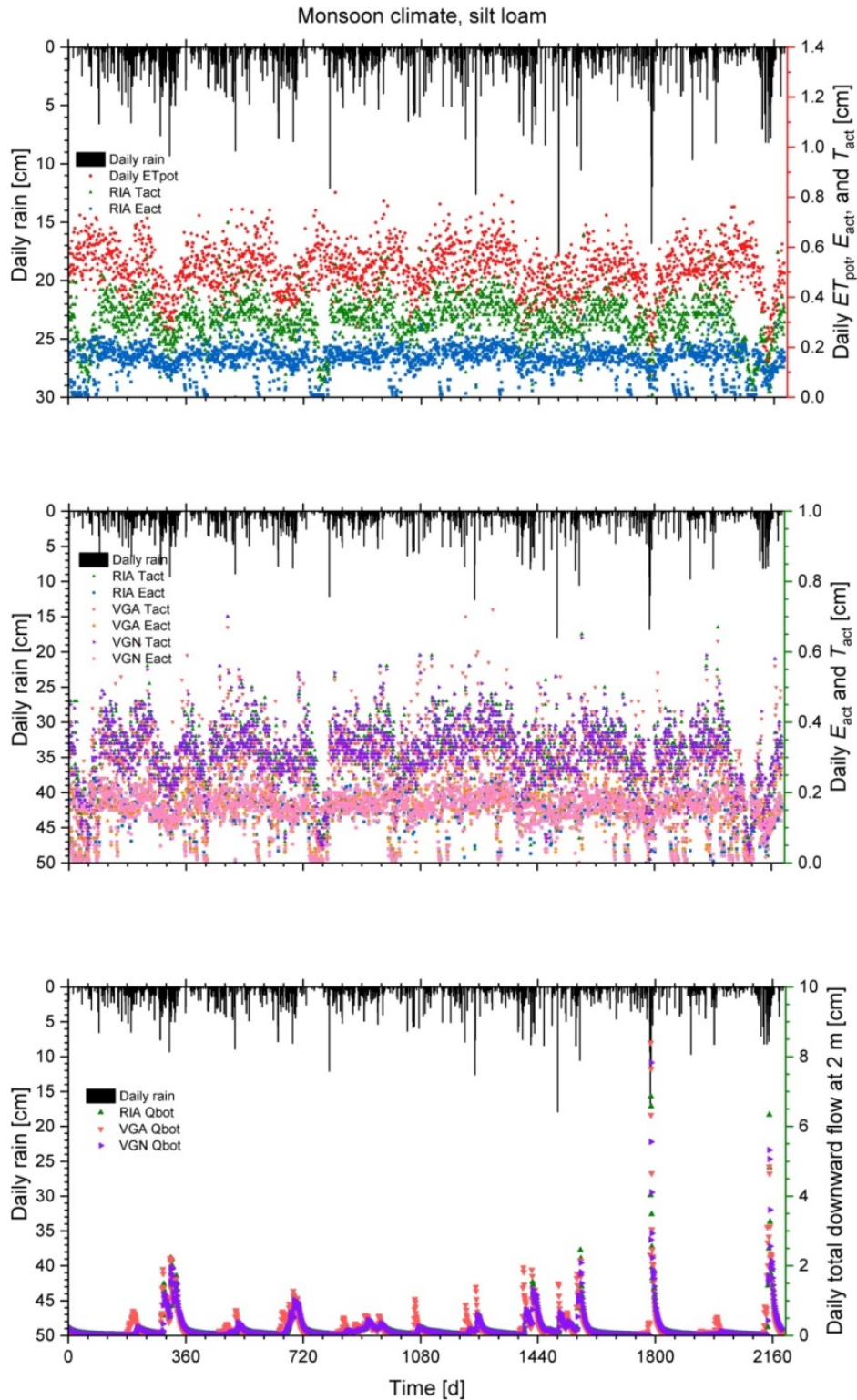
134 The silt loam had a high water holding capacity, and the reduction in T_{act} in the
135 summer was less severe than for clay (Fig. S8). Still, there were many days with strongly
136 reduced evapotranspiration rates in the second and fourth year. The dry summer periods
137 were punctuated by brief intervals of increased evapotranspiration in response to rainfall.

138 In loamy sand, the decline of T_{act} in particular was rapid and deep in late spring or
139 early summer due to the rainfall deficit that caused the root zone to dry out (Fig. S9). The
140 limited water holding capacity of this relatively coarse-textured soil made these effects
141 much more pronounced compared to the other soils: every year had a large number of
142 days with very low evapotranspiration. VGA's evapotranspiration was more sensitive to
143 the rainfall signal than that of VGA or RIA.

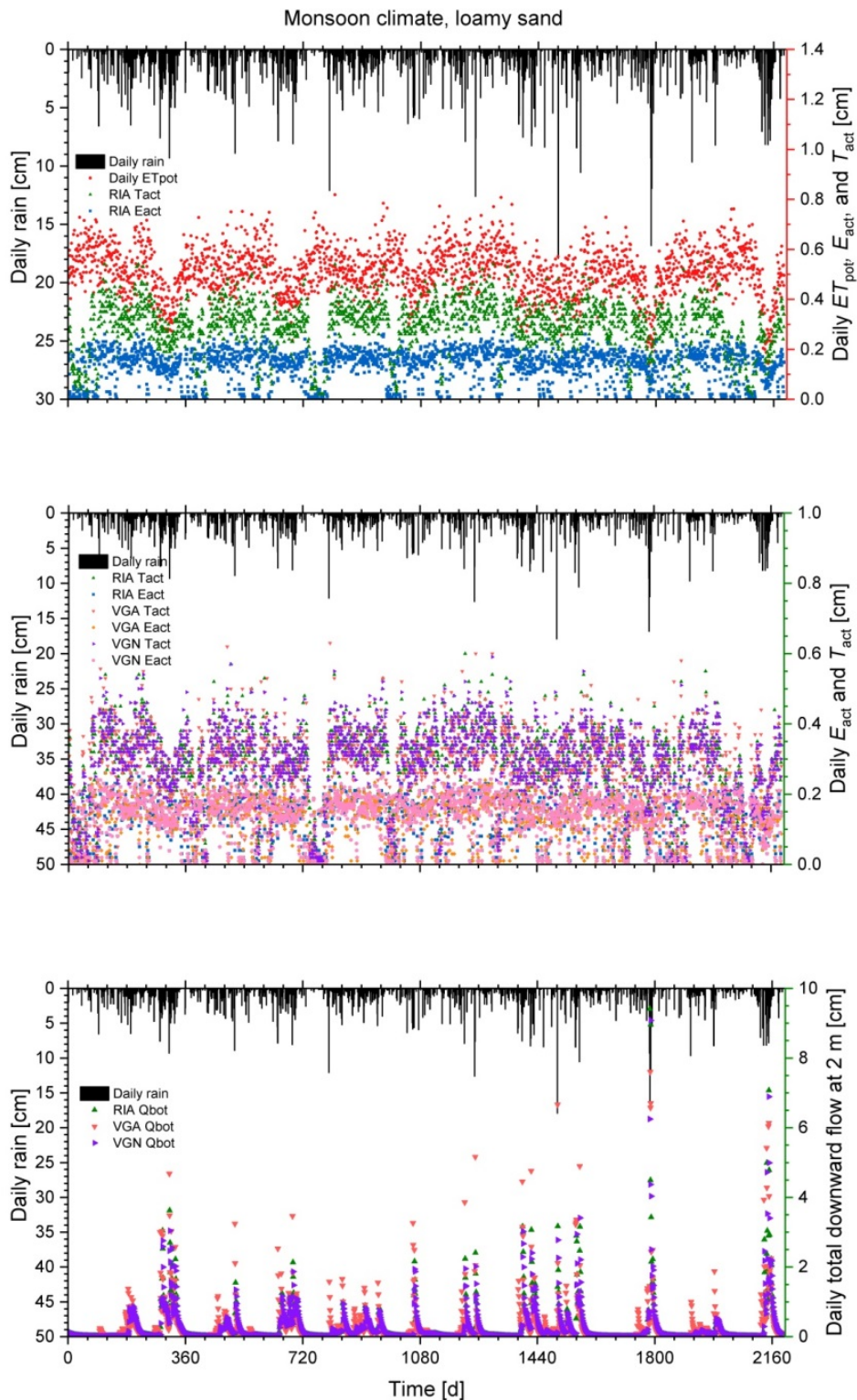
144 The rainfall excess in winter could sustain a downward flux at 2 m depth almost
145 year-round for the RIA parameterization of clay (Fig. S7). For the silt loam (Fig. S8), both
146 VGN and RIA had year-round deep drainage, while VGA showed much higher peaks
147 during wet periods that arrived well before those of VGA and RIA but dropped off much
148 faster and reached negligible values for some period of time every year. For the loamy
149 sand (Fig. S9) VGA still had the highest peak of deep drainage, but the difference in the
150 levels and arrival times of the peaks was smaller than for silt loam. Deep drainage became
151 negligible for roughly half of the time for VGA and for shorter periods for VGN and RIA.
152



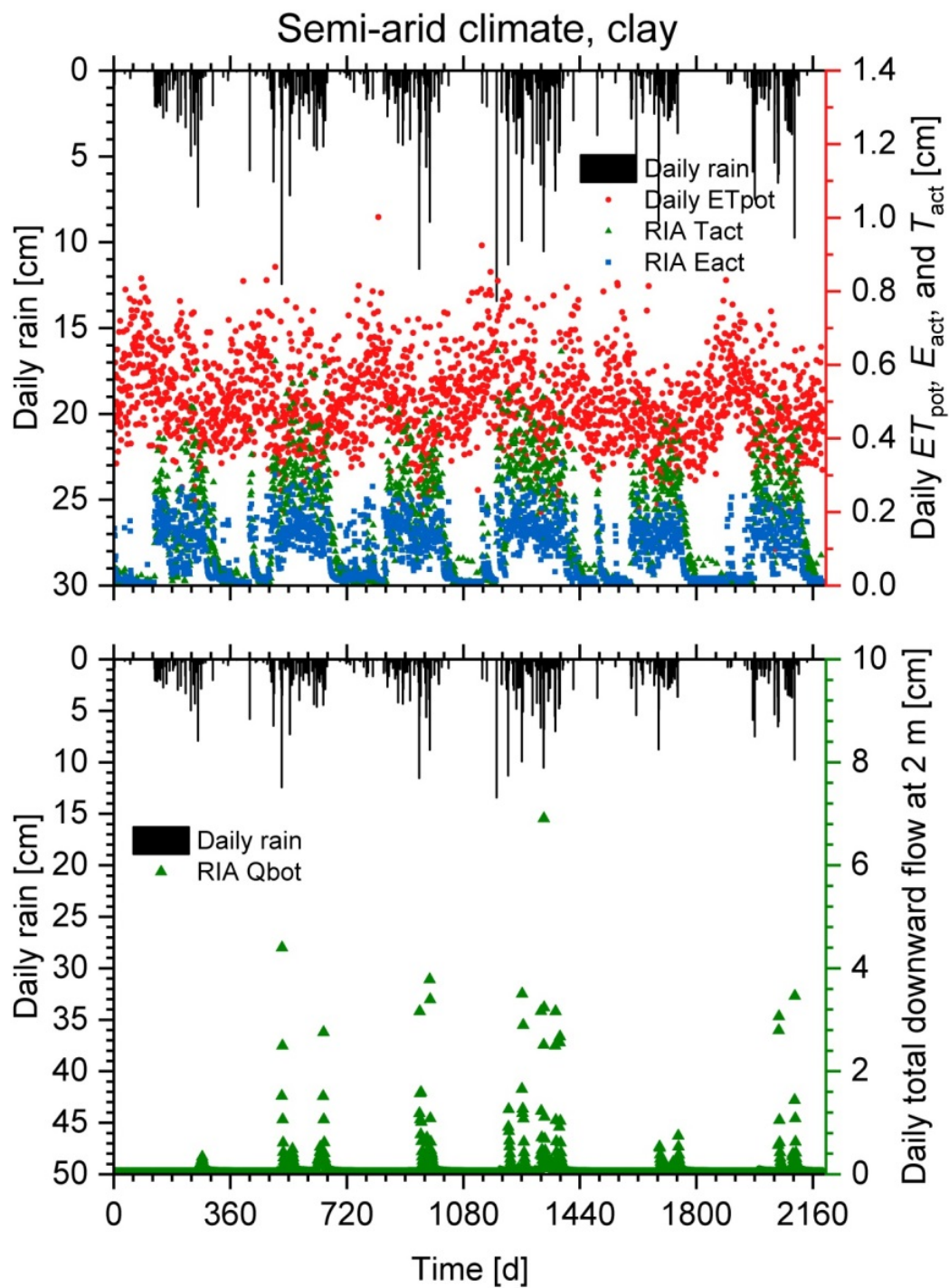
153
 154 Figure S1. Generated rainfall and potential evapotranspiration (ET_{pot}) for a monsoon
 155 climate, and the simulated actual transpiration (E_{act}) and evaporation (T_{act}) (top panel),
 156 as well as the daily downward flow at 2 m depth (bottom panel) for a clay soil. The graphs
 157 cover a six-year period starting at January 1st. The second and sixth year are leap years.
 158 Simulations results are shown for the RIA parameterization only because the other
 159 parameterizations did not run successfully. The parameterizations are explained in Fig. 1
 160 and the main text.



161
 162 Figure S2. The weather data are those of Fig. S1, but the soil is a silt loam. The top panel
 163 shows the weather data and actual transpiration (E_{act}) and evaporation (T_{act}) according
 164 to the RIA parameterization. The middle panel shows E_{act} and T_{act} for the VGN, VGA, and
 165 RIA parameterizations for comparison. The bottom panel has the downward fluxes at 2 m
 166 depth for all three parameterizations.

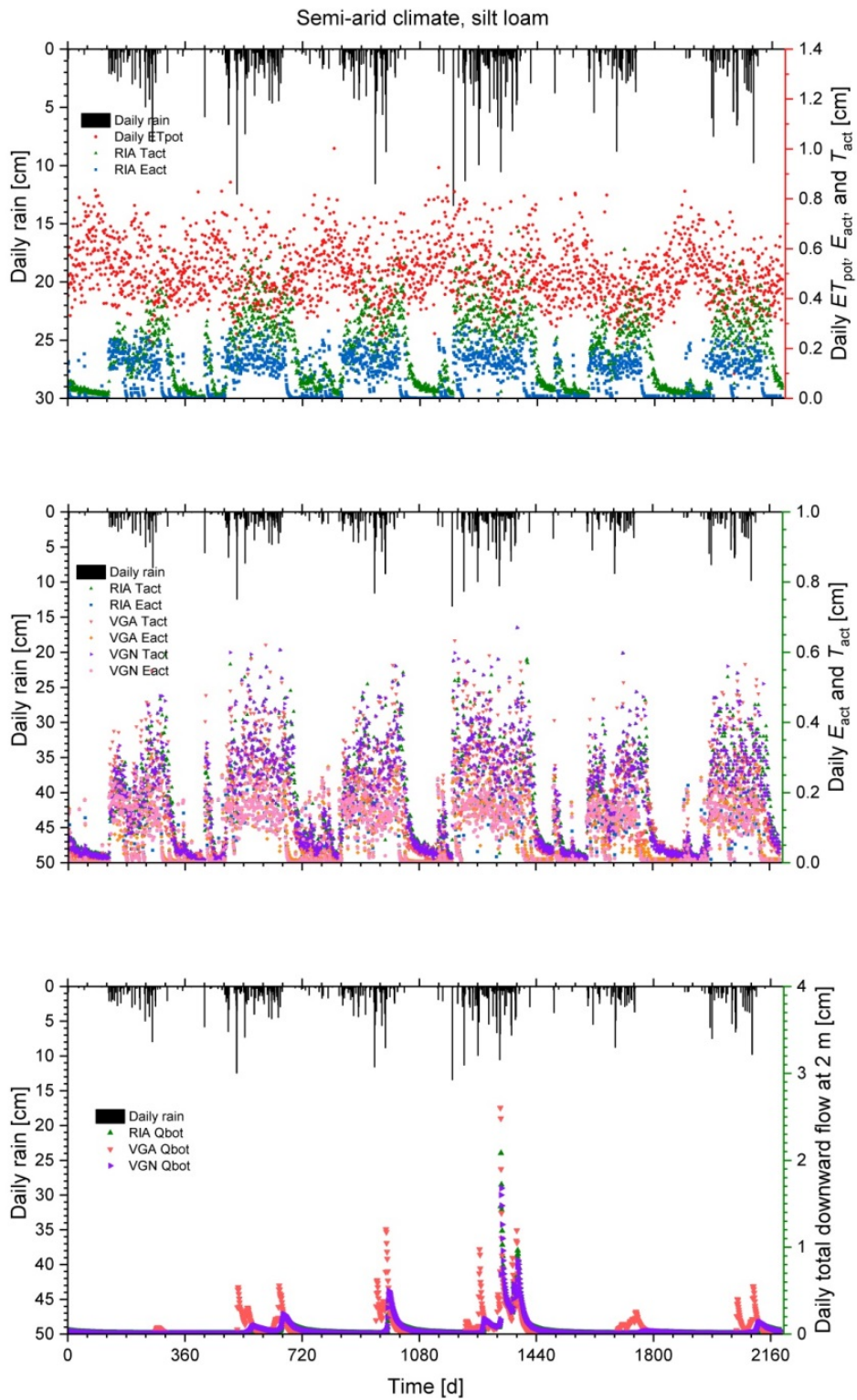


167
 168 Figure S3. The weather data are those of Fig. S1, but the soil is a loamy sand. The top panel
 169 shows the weather data and actual transpiration (E_{act}) and evaporation (T_{act}) according
 170 to the RIA parameterization. The middle panel shows E_{act} and T_{act} for the VGN, VGA, and
 171 RIA parameterizations for comparison. The bottom panel has the downward fluxes at 2 m
 172 depth for all three parameterizations.

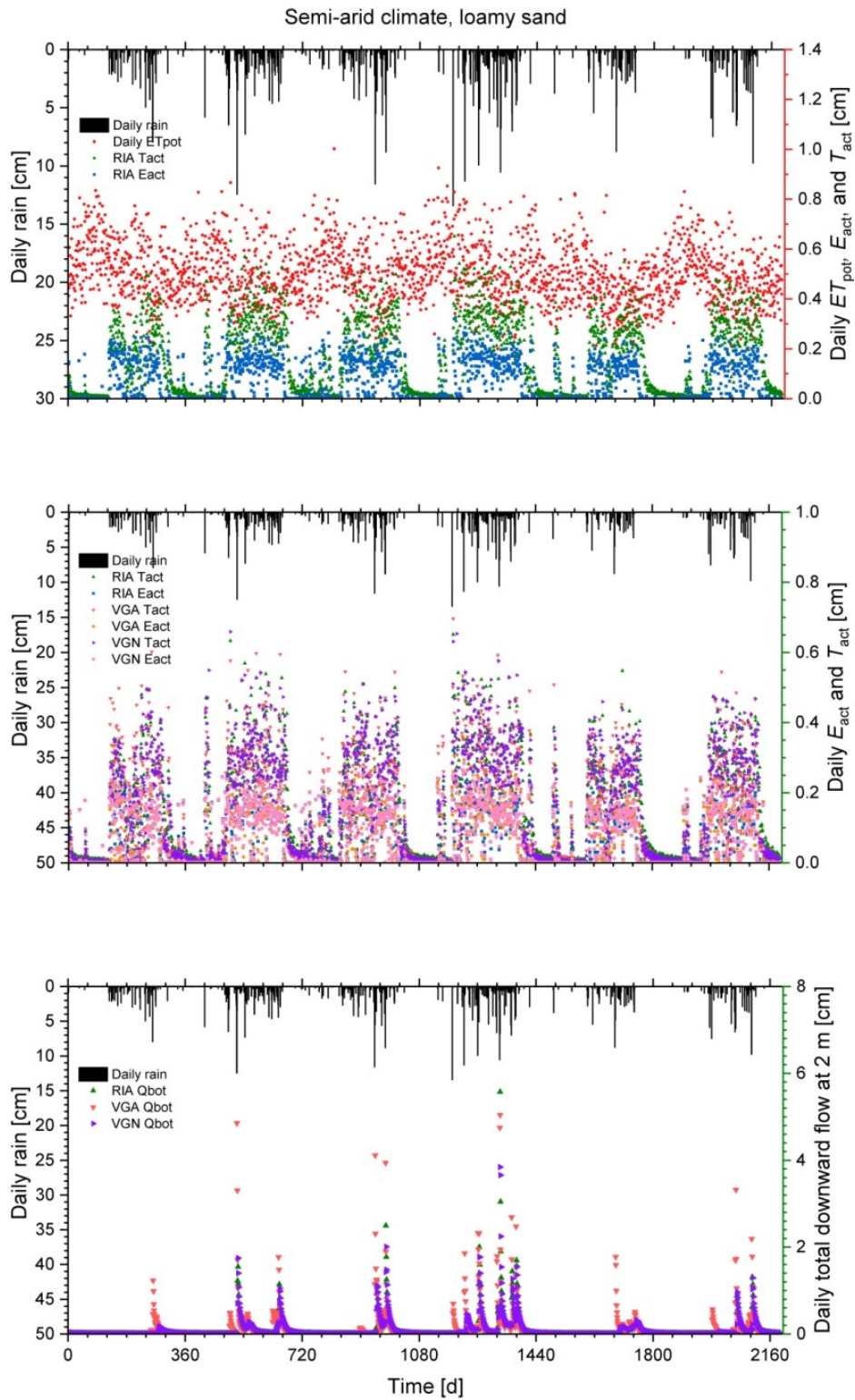


174

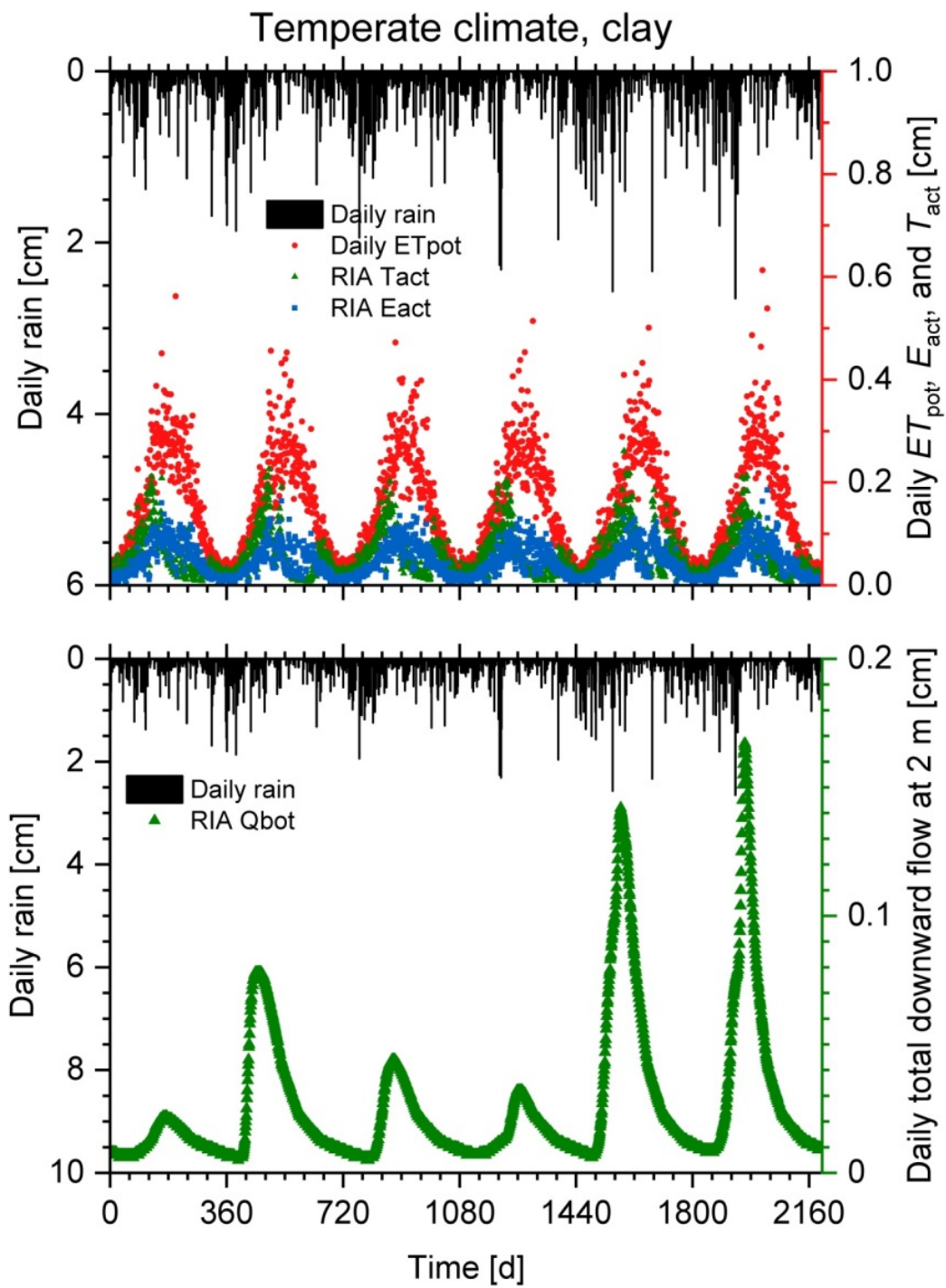
175 Figure S4. Like Fig. S1, but for a semi-arid climate.



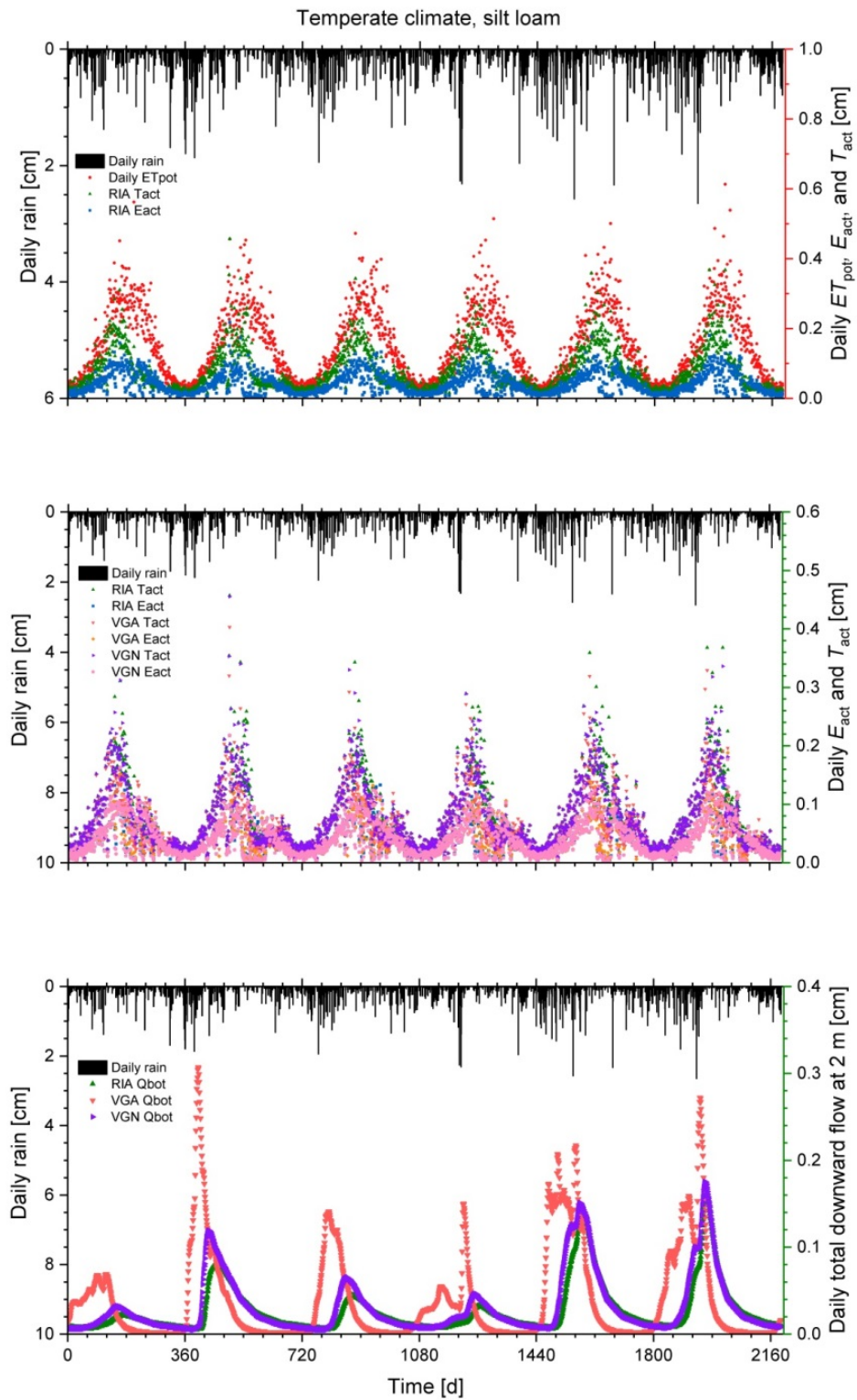
176
 177 Figure S5. Like Fig. S2, but for a semi-arid climate.
 178



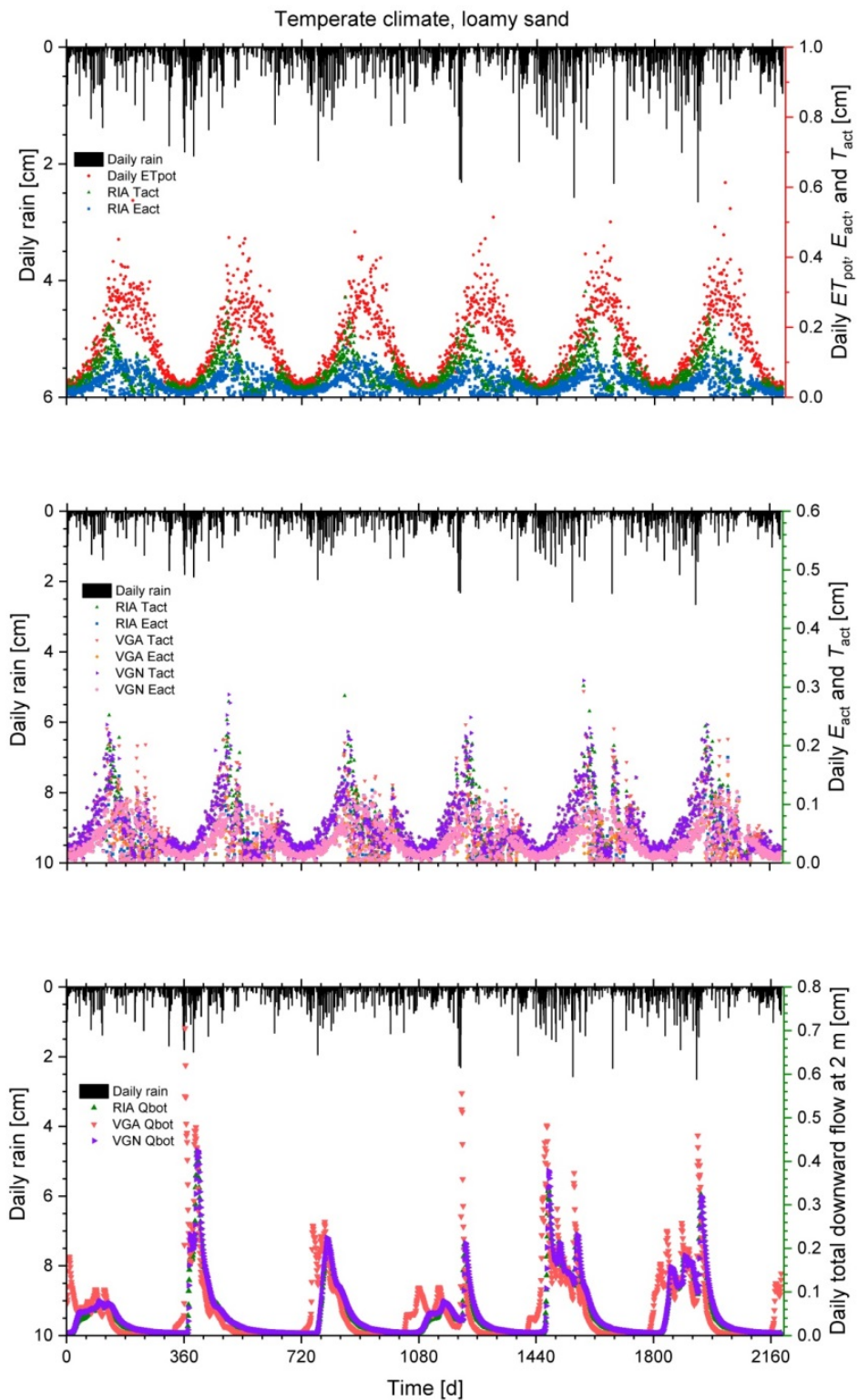
179
 180 Figure S6. Like Fig. S3, but for a semi-arid climate.
 181



182
 183 Figure S7. Like Fig. S1, but for a temperate climate.
 184



185
 186 Figure S8. Like Fig. S2, but for a temperate climate.
 187



188
 189 Figure S9. Like Fig. S3, but for a temperate climate.
 190
 191

192 **References**

193

194 Brown, R. N., Percivalle, C., Narkiewicz, S., and DeCuollo, S.: Relative rooting depths of
195 native grasses and amenity grasses with potential for use on roadsides in New
196 England, *HortScience* 45, 393–400, 2010.

197 Davies, J. A.: A note on the relationship between net radiation and solar radiation,
198 *Quarterly Journal of the Royal Meteorological Society*, 93, 109–115, 1967.

199 de Rooij, G. H.: A simple weather generator for applications with limited data availability:
200 TEmpotRain 1.0 for rainfall, temperatures, extraterrestrial radiation, and potential
201 evapotranspiration, *Geosci. Model Dev. Discuss.*, doi: 10.5194/gmd-2018-97,
202 2018.

203 Droogers, P., and Allen, R. G.: 2002. Estimating reference evapotranspiration under
204 inaccurate data conditions, *Irrigation and Drainage Systems*, 16, 33–45, 2002.

205 Evett, S. R.: Energy and water balances at soil–plant–atmosphere interfaces, in:
206 *Handbook of soil science*, edited by Sumner, M. E. editor, CRC Press, Boca Raton,
207 Fla., U.S.A., A129 – A182, 2000.

208 Grant, I. F., Prata, A. J., and Cechet, R. P.: The impact of diurnal variation of albedo on the
209 remote sensing of the daily mean albedo of grassland, *J. Appl. Meteorology*, 39,
210 231–244, doi: 10.1175/1520-0450(2000)039<0231:TIOTDV>2.0.CO;2, 2000.

211 Pham, M. T., Vanhaute, W. J., Vanderberghe, S., De Baets, B, and Verhoest, N. E. C.: An
212 assessment of the ability of Bartlett–Lewis type of rainfall models to reproduce
213 drought statistics, *Hydrol. Earth Syst. Sci.*, 17, 5167–5183, doi:10.5194/hess-17-
214 5167-2013, 2013.

215 Šimůnek, J., Šejna, M., Sait., H., Sakai, M., and van Genuchten, M. Th.: The HYDRUS–1D
216 software package for simulating the one–dimensional movement of water, heat,
217 and multiple solutes in variably–saturated media, Version 4.17, Dept. Env. Sci.,
218 Univ. Calif., Riverside, CA, U.S.A., 2013.